Quantum confinement effects on optical transitions in nanodiamonds containing nitrogen vacancies

Alessio Petrone, Joshua J. Goings, and Xiaosong Li

Phys. Rev. B **94**, 165402 — Published 3 October 2016

DOI: 10.1103/PhysRevB.94.165402

Quantum Confinement Effects on Optical Transitions in Nitrogen-Vacancy Containing Nanodiamonds

Alessio Petrone, Joshua J. Goings, and Xiaosong Li*
Department of Chemistry, University of Washington, Seattle, WA, 98195
(Dated: September 15, 2016)

Colored nitrogen-vacancy (NV) centers in nanosize diamonds (d∼5 nm) are promising probe materials, because their optical transitions are sensitive to mechanical, vibrational and spin changes in the surroundings. Here, a linear response time-dependent density functional theory approach is used to describe the optical transitions in several NV-doped diamond quantum dots (QDs) in order to investigate size effects on the absorption spectra. By computing the full optical spectrum up to band-to-band transitions, we analyze both the localized "pinned" mid-gap and the charge-transfer excitations for an isolated reduced NV center. Sub-band charge-transfer excitations are shown to be size dependent, involving the excitation of the dopant sp^3 electrons to the diamond conduction band. Additionally, the NV-doped systems exhibit characteristic $sp^3 - sp^3$ excitations whose experimental energies are reproduced well and do not depend on QD size. However, the NV position and global cluster symmetry can affect the amount of the energy splitting of the vertical excitation energies of the mid-gap transitions.

I. INTRODUCTION

Pure diamonds are excellent insulators with a large optical band gap (∼5.5 eV)[1]. They are transparent to visible radiation, but introducing defects (dopants) can selectively change their optical properties. The influence of dopants on optical properties may be further modulated by adjusting the host nanocrystal size. As nanocrystal cluster size decreases, discrete electronic levels emerge at band edges. Frontier orbitals separate energetically and a simultaneous band gap increase is observed.[2–7] These are all consequences of the quantum confinement effect.[8–11] As a result, the electronic properties of doped semiconductor nanocrystals can be experimentally tuned, making them suitable candidates for many technological applications.[12–18]

For diamond, nitrogen is an extremely common impurity and nitrogen-vacancy (NV) color centers have received attention for their sensitive optical and spin properties. The NV center can exist as either a neutral doublet in its ground state, $^2NV^0$, or an anionic state that may be either a singlet, $^1NV^-$, or triplet, $^3NV^-$. The latter is the most common stable ground state electronic configuration[19–22]. As NV-containing diamond approaches the nanosize (d∼ 5 nm), they show promise for many technological applications, such as quantum computing[23], ultra-sensitive magnetometry[24], and biolabeling[25,26]. Doping may introduce new sub-band-gap levels, and diamond NV centers in particular introduce new dopant-centered $sp^3 - sp^3$ mid-gap electronic transitions and charge-transfer (CT or "photoionization") excited states. The latter may also be affected by the system size, and in doped semiconductor nanocrystals quantum confinement effects have been observed to shift the band edges relative to energetically pinned levels, resulting in diameter-dependent CT energies.[27,28]

Despite the importance of the optical and CT transitions in NV doped diamonds, the electronic structure of NV color centers in nanodiamond quantum dots (QDs) has not been well studied[29]. In particular, the effects of the NV center position (i.e. surface effects, symmetry breaking) and size (i.e. quantum confinement) on the electronic excitations are not well characterized. Within the context of density functional theory (DFT), electronic excitations are often approximated as the difference between orbitals energies. Many previous theoretical studies of NV-doped diamond have relied on the orbital energy difference approach to compute electronic excitations. While appropriate for some cases, a more accurate approach that includes some orbital relaxation upon the excitation is required. Furthermore, these studies have relied on periodic boundary conditions, which cannot easily or accurately capture quantum confinement effects on optical properties of NV-containing nanodiamonds.[19,21,30–37] Conversely, while linear response time dependent density functional theory (LR-TDDFT) along with multi-reference methods (i.e. CASSCF, MRCI, CASPT2) can provide more accurate results for excitation energies, relatively few computational studies on NV centers in nanodiamonds have been performed. In these cases, the systems under investigation have been strongly size limited (less then 100 atoms), due to the very high computational cost.[38–40] Here we present a theoretical analysis of the electronic properties of a reduced isolated NV color center in nanodiamond QDs combining TDDFT with a finite cluster approach. This technique has shown very promising results in our lab for the theoretical characterization of the excited states in doped semi-conductor quantum dots.[28,41–46] Using this technique on a broad range of NV-diamond QD sizes, we explore quantum confinement effects on the highly localized mid-gap transitions, as well as the higher energy CT states. Because CT transitions are broad and show strong spectral overlap with many other optical features, this theoretical method is strongly motivated by the desire to disentangle the full range of electronic transitions in NV-doped nanodiamond.

II. METHODOLOGY

Nearly spherical nano-diamonds quantum dots, $C_{44}H_{42}$ (diameter ∼0.8 nm), $C_{121}H_{104}$ (diameter ∼1.2 nm), $C_{182}H_{142}$ (diameter ∼1.4 nm), and $C_{487}H_{310}$ (diameter ∼2.1 nm) were constructed (see Fig. 1) using the bulk face-centered cubic lattice parameter[1] $a_0 = 0.357$ nm. Each QD has a C_{3v} symmetry in the absence of the NV center. Hydrogen atoms were used to passivate the surface carbon atoms and to saturate surface dangling bonds. The sizes of these three QDs are similar to the smallest nano-diamonds obtainable by detonation synthesis.[47–49] As the diamond excitonic Bohr radius is estimated to be ∼1.6 nm,[50] electronic properties of these small diamond QDs will exhibit quantum confinement effects.

All calculations were performed using the the development version of Gaussian software package.[51] The ground state electronic structures were obtained by solving the Kohn-Sham equation using the hybrid B3LYP functional.[52–54] We also compared the optical spectra computed using the long-range corrected (LC-) version[55] of the BLYP[53,54,56] functional with those computed with B3LYP. Results show that although characteristics of the spectra computed with LC-BLYP and B3LYP are similar, the LC-BLYP band gaps are strongly blue shifted compared to the experimental values. On the other hand, B3LYP results show a much better agreement with experiment. The electronic structures of excited states were calculated using the time-dependent DFT (TDDFT) within the linear response framework.[57–59] and its energy specific implementation for the high energy states[60,61]. Diffuse functions have been previously shown to be unimportant for clusters whose diameter is larger than 1 nm[39]. Despite this, we also checked the effect of the diffuse functions for the NV center atoms for the 1.2 nm cluster, and did not observe any significant change in the vertical excitation energy (data not shown). For these reasons the 6-31G(d) basis set has been used within this study.

The NV center was created by replacing a carbon atom with a nitrogen atom near the center of the QD, followed by eliminating one of its neighbor carbon atom along the C_{3v} axis of the model. To avoid the insufficient description of the vacancy, a ghost atom (no nuclear charges or electrons) with 6-31G(d) basis functions was defined at the center of the vacancy. To evaluate the lattice distortion due to the presence of the NV center itself, the NV center and the nearest neighboring six carbon atoms were fully optimized while maintaining the rest of the diamond structure at the crystal lattice. In this study we focused on the reduced NV center, whose ground state has been shown to be a triplet.[19–21]

III. RESULTS AND DISCUSSION

A. Ground State Structure and Energy Levels

The lattice structural reorganization upon doping NV in nanodiamond is summarized in Fig. 2, where the average bond length changes (in percentage) of the atoms close to the vacancy are presented. All nanocrystals show a ∼ 1% CC bond (1.52 Å average bond length) contraction around the NV center compared to bonds (1.54 Å average CC bond length) in NV-free nanocrystals. A larger reorganization for the CN bond (1.48 Å average bond length) is observed due to the larger electronegativity of the nitrogen.

Figure 3 shows the total and partial density of states (PDOS) using the calculated molecular orbitals, with the spin-up and spin-down density plotted as positive and negative values, respectively. Both the valence band (VB) and conduction band (CB) consist of carbon p and s characters, while multiple levels at the NV center appear inside the band-gap. The VB and CB of the ∼2.1 nm diameter nanodiamond are separated by a HOMO-LUMO energy gap of 5.82 eV. As the size of nanodiamond decreases, this gap increases due to stronger quantum confinement effects. For the ∼0.82 nm nanodiamond, the energy gap is 7.70 eV.

The nitrogen atom contributes three electrons to three C-N valence bonds embedded in the VB, leaving a lone-pair of valence electrons to the NV center. There are three dangling electrons from three nearest neighboring C atoms to the vacancy, giving rise to a total of 5 electrons at the NV center (6 for the reduced system). Due to the presence of the NV center, the local crystal symmetry becomes C_{3v} (instead of T_d) along the N-V bond. In this local C_{3v} symmetry, the four sp^3 orbitals are grouped into two e orbitals (e_x, e_y) and two a orbitals (a_1 and a_1'), schematically illustrated in Fig. 4. Orbitals with a_1 symmetry shown in Fig. 4 are σ-bond like and are localized at the N-V bond with significant contributions from the nitrogen p. In the 2.1 nm nanodiamond, the a_1' orbital of the NV center energetically overlap with the VB edge. As the QD size decreases, the VB edge red-shifts due to the quantum confinement. The a_1 and a_1' levels are mostly energetically "pinned", i.e. their energies relative to the Fermi level are constant. As a result, in smaller nanodiamonds, a_1' orbitals are well separated from the VB. Both a_1 and a_1' orbitals consist of contributions from nitrogen p. Orbitals with e symmetry shown in Fig. 4 are mostly localized at the vacancy center, and are also energetically "pinned" inside the band-gap. Based on Fig. 4, it is clear that the anionic NV-containing nanodiamonds have a triplet ground state (two unpaired electrons occupying two different e orbitals) whereas all a_1 orbitals are doubly occupied.

This unique electronic structure gives rise to several characteristic sets of optical transitions exhibited in spectroscopic measurement of NV-containing nanodiamonds. Optical spectra for the NV^- triplet computed using lin-

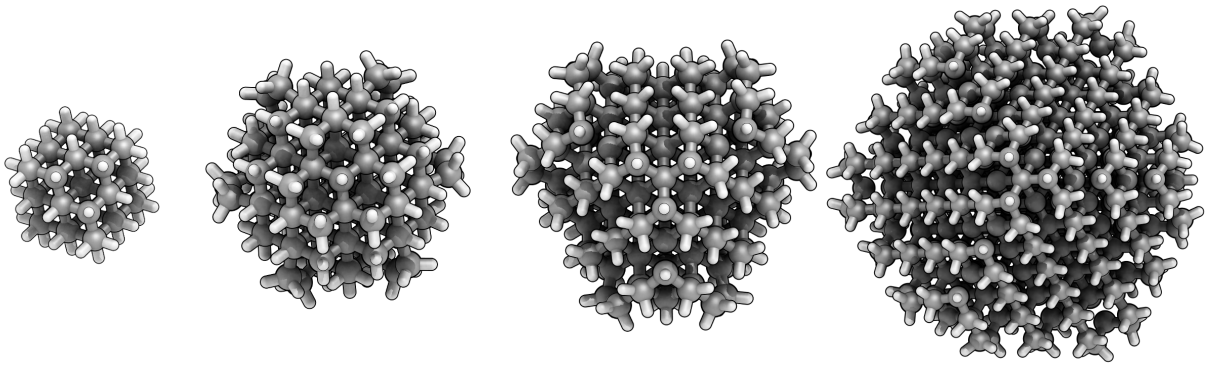

FIG. 1. Top view of pure nanodiamond ball and stick models, carbon in gray and hydrogen in white. The $C_{44}H_{42}$ (diameter ∼0.8 nm), $C_{121}H_{104}$ (diameter ∼ 1.2), $C_{182}H_{142}$ (diameter ∼1.4 nm) and $C_{487}H_{310}$ (diameter ∼2.1 nm) are represented from left to right with the C_{3v} axis entering in the plane of the figure.

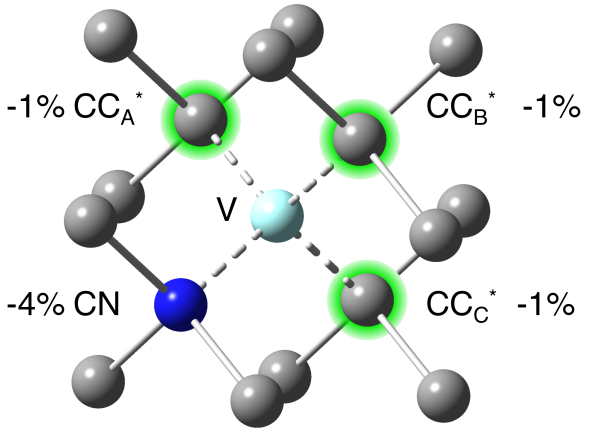

FIG. 2. Geometry relaxation near the NV center: carbon in grey, nitrogen in blue and the vacancy is in light blue.

	Diameter (nm)	E_g^{TD} (eV)	$E_g^{HOMO-LUMO}$ (eV)
$C_{44}H_{42}$	0.82	7.04	7.70
$C_{121}H_{104}$	1.25	6.01	6.50
$C_{182}H_{142}$	1.43	5.86	6.27
$C_{487}H_{310}$	2.05	5.54	5.82

TABLE I. Diameter (nm) and band gap (eV) values, these last ones both evaluated as TD-B3LYP/6-31G(d) optical band to band excitation, E_g^{TD}, and as the difference between the LUMO and HOMO energies, $E_g^{HOMO-LUMO}$.

ear response TDDFT are reported in Fig. 6. The following discussion will focus on illustrating the physical nature of these transitions and the effects of quantum confinement.

B. VB → CB Transitions

VB → CB transition frequency in nanodiamond is independent of the presence of the NV center. However, the intensity of the optical gap transition is reduced compared to the NV-free nanocrystal because there are fewer carbon atoms that contribute to the optical gap transitions in NV-containing nanodiamond. The TDDFT computed optical band-gaps E_g of pure (NV-free) nanodiamonds as a function of dot size are plotted in Fig. 5 and listed in Table I. The diamond excitonic Bohr radius is estimated to be ∼1.6 nm (diameter ∼3.2 nm).[50] Clearly, the QDs used in this work are within the quantum confinement regime. As the size of nanodiamond decreases, the quantum confinement effect[11,62] leads to an increase in the band-gap (5.54 eV for C_{487}, 5.86 eV for C_{182}, 6.01 eV for C_{121} and 7.04 eV for the C_{44}), similar to that observed in semiconducting nanocrystals.[28,63] For spherical QDs with radius r, the correction to the energy of the excitonic transition, $\Delta E_{EXC} = E_{EXC}(r) - E_g(r = \infty)$, depends on the quantum confinement terms and the Coulomb interaction between the electron and hole, as described by the well-known equation[10,28,64,65]:

$$E_{EXC}(r) \approx \frac{\hbar^2\pi^2}{2r^2}\left[\frac{1}{m_e^*} + \frac{1}{m_h^*}\right] - \frac{1.8e^2}{\epsilon r} + E_g(r = \infty) \quad (1)$$

where m_e^* and m_h^* are the effective masses (in units of electron mass) of the electron and hole in pure diamond QDs, respectively, e is the electron charge, $\hbar$ is Plancks constant, and ϵ is the dielectric constant. Extrapolation to the bulk limit according to Eq. (1) results in a bulk band gap of ∼5.5 eV, in excellent agreement with

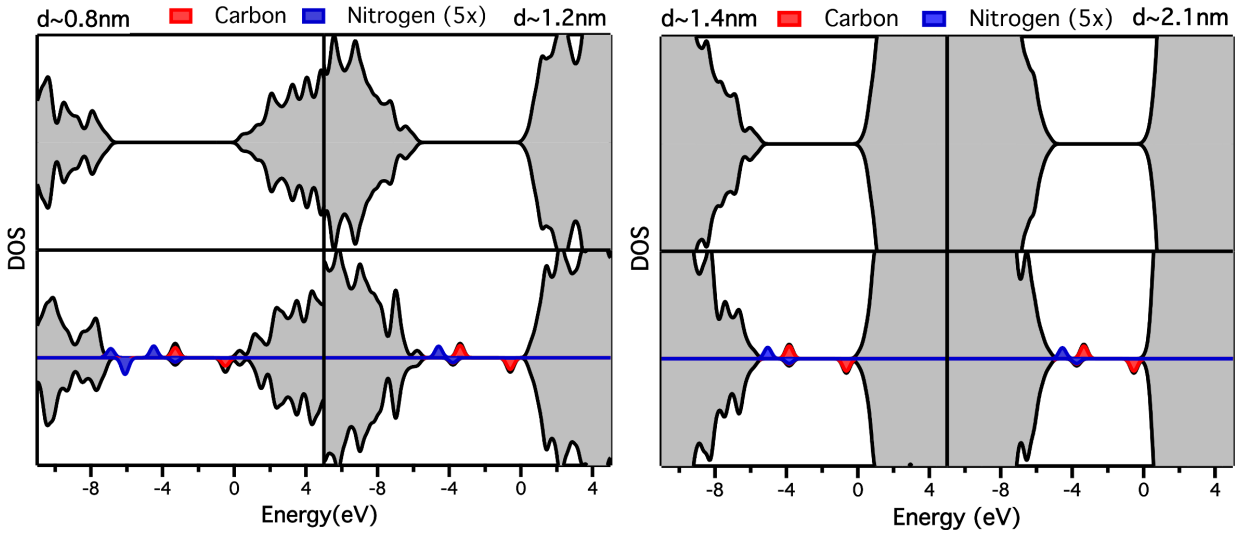

FIG. 3. B3LYP/6-31G(d) DOS and PDOS (this last visualized only for the level within the band gap). The red and blue colored regions show the C p and N p (magnified by 5x) contributions to the PDOS diagram, respectively. Spin-up, positive density values; spin down, negative density values. The DOS diagram are calculated for the pure C_XH_Y , and the reduced $^3NV^-$ $C_{X-2}NH_Y$ (from top to bottom) relaxed nanodiamonds of increasing sizes (d$\sim$ 0.8, 1.2, 1.4, and 2.1 nm from left to right).

the literature value of $\sim$5.5 eV[1] of the bulk optical band gap. The observed quantum confinement effect in these nanodiamonds suggests that charge transfer transitions between diamond bands and levels at the NV center are modulated by the size of the nanodiamond.

C. Mid-Gap NV-centered Optical Transitions

The energy levels of the NV-center in diamond lattice are illustrated in Fig. 4. The presence of these levels leads to unique mid-gap optical transitions of NV-containing nanodiamonds. The optical absorption spectrum of C_{180} nanocrystal in Fig. 6 shows that the NV $\rightarrow$ NV excitations appear below the band gap transition. The isolated peak at 2.23 eV consists of two degenerate transitions, $a_1(\beta) \rightarrow e_x(\beta)$ and $a_1(\beta) \rightarrow e_y(\beta)$. These transitions give rise to the experimental zero phonon line (ZPL) of $^3A_2(a_1^2e^2) \rightarrow {}^3E(a_1e^3)$ excitation at 1.945 eV.[20–22,66] Our value for the vertical excitation energy (VEE) is $\sim$0.28 eV higher than the experimental ZPL, but in good agreement with recent calculations and experimental studies including the Frank-Condon shift of $\sim$0.25 eV, due to the structural reorganization in the excited state (included in the ZPL and neglected in the VEE).[22,33,66–68] Because these transitions are symmetry allowed, they exhibit non-zero oscillator strengths. The second NV $\rightarrow$ NV absorption peak, which corresponds to degenerate $a_1'(\beta) \rightarrow e_x(\beta)$ and $a_1'(\beta) \rightarrow e_y(\beta)$, appears at 4.9 eV, inside the charge-transfer excitation band.

Table II lists the energetics of VEEs in various NV-containing nanodiamonds. As the energy levels of the NV-center are energetically "pinned", electronic excitations among these levels are largely independent of the size of the nanodiamond and the quantum confinement effect. The smallest nanodiamond is not considered here because the geometry relaxation near the NV center involves mostly surface carbon atoms. The effect of lattice reorganization on the VEE is estimated to be 70 meV. This value is obtained by comparing the VEE spectra computed with frozen lattice and relaxed lattice, where the NV center and neighboring six carbon atoms are fully optimized. A very small ZPL spectral splitting of $\sim$0.3 meV has been observed experimentally, although this values varies between center to center.[21,37] However, for NV

	NV relaxed	NV frozen
$^3NV^-$ $C_{119}NH^-_{104}$	2.23 (0.05)	2.30 (0.04)
	2.23 (0.05)	2.30 (0.04)
$^3NV^-$ $C_{180}NH^-_{142}$	2.23 (0.05)	2.30 (0.04)
	2.23 (0.05)	2.30 (0.04)
$^3NV^-$ $C_{485}NH^-_{310}$	2.22 (0.05)	2.29 (0.04)
	2.22 (0.05)	2.29 (0.04)

TABLE II. TD-B3LYP/6-31G(d) mid-gap vertical excitation energies (a_1 to e, beta manifold) for the $^3NV^-$ systems (in eV) and the corresponding oscillator strengths (reported in parenthesis). We compare results between the NV relaxed (NV center position is optimized, see text) with the one obtained just inserting the NV center by replacing the corresponding atoms (NV frozen) in the pure nanodiamond.

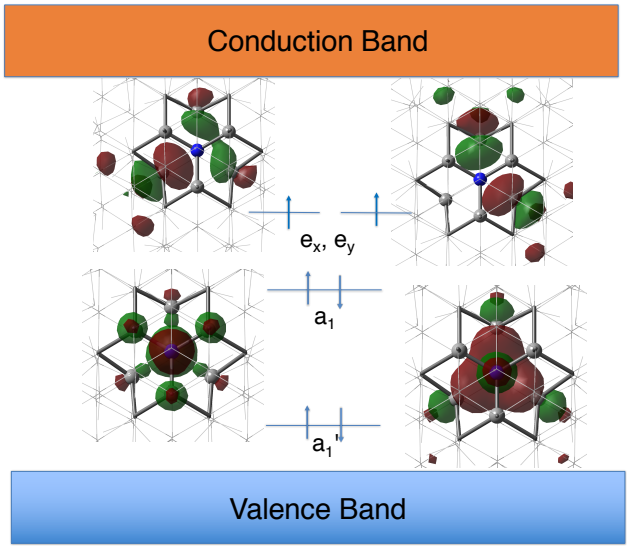

FIG. 4. Schematic illustration of the NV center electronic configuration, according to the C_{3v} point group symmetry. From a theoretical point of view the two sets of e MOs are energetically equivalent in a completely symmetric environment. The two a MOs above the valence band are completely filled and for the anionic tripled two additional electrons are placed in the e MOs as well. The zoomed in $C_{180}NH_{142}$ B3LYP/6-31G(d) alpha MOs contour plots with the pseudo C_{3v} axis parallel to the z-axis (entering the figure) and using the 0.05 isodensity value are also represented.

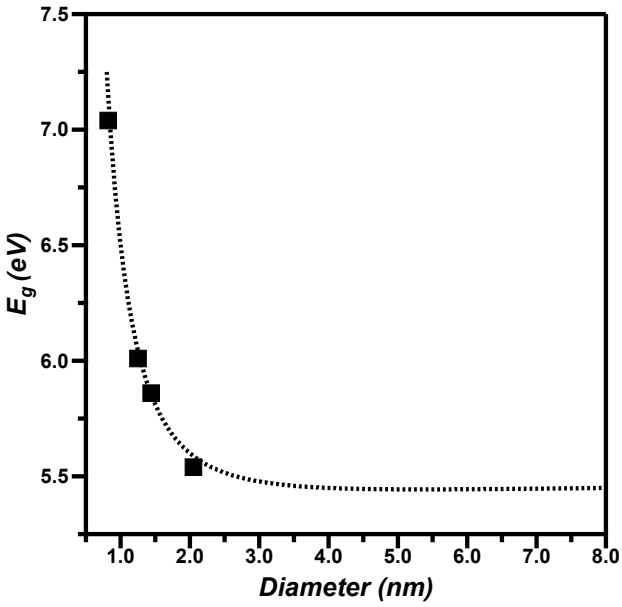

FIG. 5. TDDFT optical band gaps (eV), squares, for the pure carbon nanodiamonds as function of the QD increasing diameter (0.82, 1.25, 1.43, 2.05 nm). The fit according to Eq. (1) is used to extrapolate the bulk band gap and is reported as well (dotted line).

center with the C_{3v} symmetry, the two first mid-gap transitions are degenerate as shown in Table II. Therefore, VEE splitting can only be a result of symmetry breaking at the NV center. This can arise from nanocrystalline anisotropy, lattice strain or surface effect. In this work, we investigate how geometric asymmetry in nanocrystal affects the NV centered optical transitions. As the NV center moves away from the C_{3v} symmetry center, its global symmetry is no longer C_{3v}. As a result, energetically degenerate e levels in the C_{3v} symmetry, as shown in Fig. 4, are no longer degenerate due to the anisotropic surface effect as the NV moves closer to surface (e.g. positions 2-4 shown in Fig. 7). Symmetry breaking of the NV center also gives rise to asymmetric distributions of electron density, shown in Fig. 8. The consequence of the symmetry breaking on VEEs is presented in Table III. A splitting of 60 meV of NV centered mid-gap transitions is observed when NV is moved away from the C_{3v} center of the nanocrystal. The magnitude of the splitting increases to 240 meV for the NV position closest to the surface. As the VEE splitting is sensitive to the geometrical distortion of the system, they can be effective probes of the global and local distortions, i.e. a mechanical stress or pressure. A comparable symmetry breaking effect could also manifest by applying anisotropic lattice strain or introduce non-spherical shape of nanocrystals. Our findings are indeed in agreement with the expected energy splitting in presence of a geometrical strain or pressure.[69–71]

	NV relaxed	NV frozen
Position 1	2.23 (0.05)	2.30 (0.04)
	2.23 (0.05)	2.30 (0.04)
Position 2	2.21 (0.05)	2.28 (0.04)
	2.27 (0.06)	2.34 (0.04)
Position 3	2.20 (0.05)	2.26 (0.04)
	2.26 (0.06)	2.32 (0.04)
Position 4	2.02 (0.05)	2.21 (0.04)
	2.26 (0.07)	2.35 (0.05)

TABLE III. TD-B3LYP/6-31G(d) NV centered mid-gap vertical excitation energies (a_1 to e, beta manifold) for the $^3NV^-$ systems (in eV) and the corresponding oscillator strengths (reported in parenthesis) as function of the NV center position moving from the center (position 1) towards the surface (position 4) for the $C_{180}NH_{142}$ system. Results are compared between the NV relaxed (NV center position is optimized, see text) with the one obtained just inserting the NV center by replacing the corresponding atoms (NV frozen) in the pure nanodiamond.

D. Charge-Transfer Transitions

The NV to conduction band (CB) charge transfer excitations also appear below the band-gap, but are higher

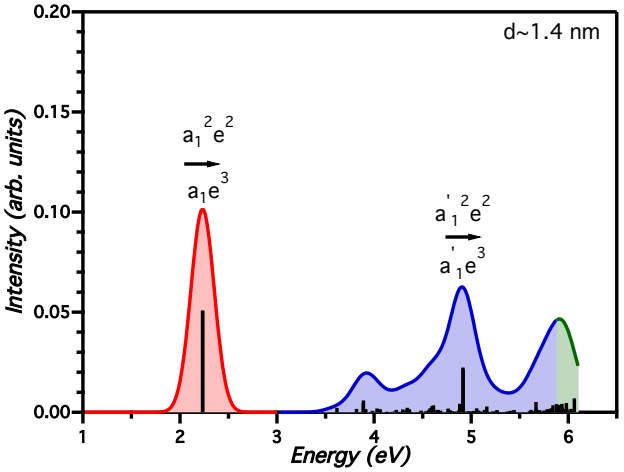

FIG. 6. TD-B3LYP/6-31G(d) optical spectrum for the relaxed $C_{180}NH_{142}$ anionic triplet system, obtained with a Gaussian smoothing function (width 0.12 eV). Three main regions are identified, the mid-gap NV centered (colored in red and/or labeled with an arrow), charge-transfer transitions (grouped together in blue) and the band to band transitions (in green); VEEs are also reported as black vertical sticks.

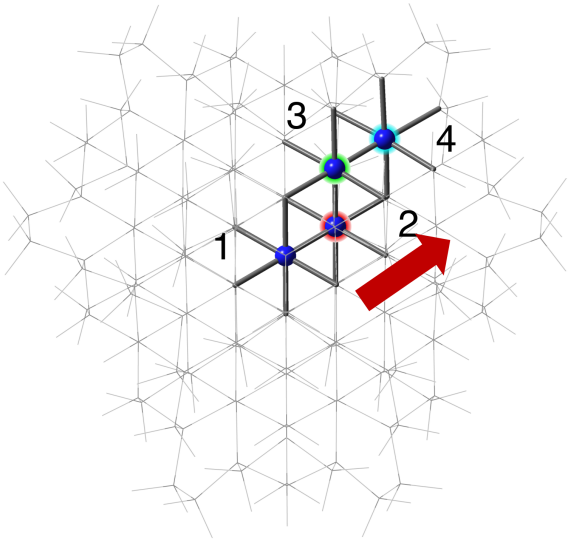

FIG. 7. Four different NV center positions in the reduced $C_{180}NH^{-}_{142}$ are investigated for anisotropic effect on NV centered optical transitions.

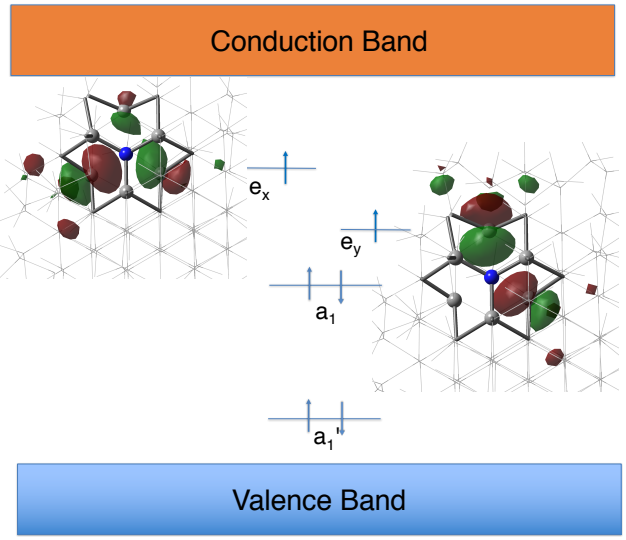

FIG. 8. Schematic illustration of the NV center electronic layout, for the position 3 NV defect that partially breaks the group symmetry. The two sets of e MOs are now not energetically equivalent anymore. The zoomed in $C_{180}NH_{142}$ B3LYP/6-31G(d) alpha MOs contour plots with the pseudo C_{3v} axis parallel to the z-axis (entering the figure) and using the 0.05 isodensity value are also represented.

	NV relaxed	NV frozen
$^3NV^-$ $C_{44}NH^-_{42}$	3.79	3.90
	3.79	3.90
$^3NV^-$ $C_{119}NH^-_{104}$	3.67	3.73
	3.67	3.73
$^3NV^-$ $C_{180}NH^-_{142}$	3.62	3.67
	3.62	3.67
$^3NV^-$ $C_{485}NH^-_{310}$	3.64	3.68
	3.64	3.68

TABLE IV. TD-B3LYP/6-31G(d) NV to CB (e to CB, alpha manifold) excitation energies for the $^3NV^-$ systems (in eV) and the corresponding oscillator strengths (reported in parenthesis). We reported results for the $C_{44}NH_{42}$, $C_{119}NH_{104}$, $C_{180}NH_{142}$, and $C_{485}NH_{310}$ systems (from top to bottom). Results are compared between the NV relaxed (NV center position is optimized, see text) with the one obtained just inserting the NV center by replacing the corresponding atoms (NV frozen) in the pure nanodiamond.

in energy than the first NV-centered transitions. This broad spectral feature starts from ∼3.6 eV and extends to the band-gap transition region (Fig. 6). The CT spectral band consists of excitations from NV-centered a_1 and e levels to the CB of diamond. At higher energetic values (∼4.6 eV) the VB to NV (empty beta e levels) excitation start to appear in the spectrum, and therefore the spectrum from 4.6 has a mixing of CT transition involving both VB to NV and/or NV to CB. Because the CB of nanodiamond is strongly affected by the quantum confinement effect, the NV to CB transitions are also modulated by the size of the nanocrystal. The quantum confinement effect on the spectral shift of the CT excitations, ΔE_{CT}, as function of the band-to-band-excitonic transition, ΔE_{EXC}, has the approximate relationship, according the effective mass approximation for a spherical

nanocrystal:[10,28,43]

$$\Delta E_{\mathrm{CT}} \approx \frac{m_e^{*-1}}{m_e^{*-1} + m_h^{*-1}} \Delta E_{\mathrm{EXC}} \quad (2)$$

where m_e^* and m_h^* are the effective masses (in units of electron mass) of the electron and hole in the NV-containing nanodiamond. The first NV to CB excitations (Table IV) as a function of the band-to-band-excitonic transition for the different dot sizes is plotted in Fig. 9. The $\Delta E_{\mathrm{CT}}/\Delta E_{\mathrm{EXC}}$ value is 0.13 and is significantly smaller than than those for the free CB electron in diamond QDs. This suggests that the photoexcited electrons in the CT excited states of NV-containing diamonds are "heavier" than those in the pure diamonds excitonic states. The shifts of the NV to CB transitions caused by the quantum confined effect are not as steep as those for the VB to CB transitions. Such behavior is expected when CT transition originates from a "pinned" NV localized level because the size dependence of the CT excitation energy comes from just one of the two diamond bands.

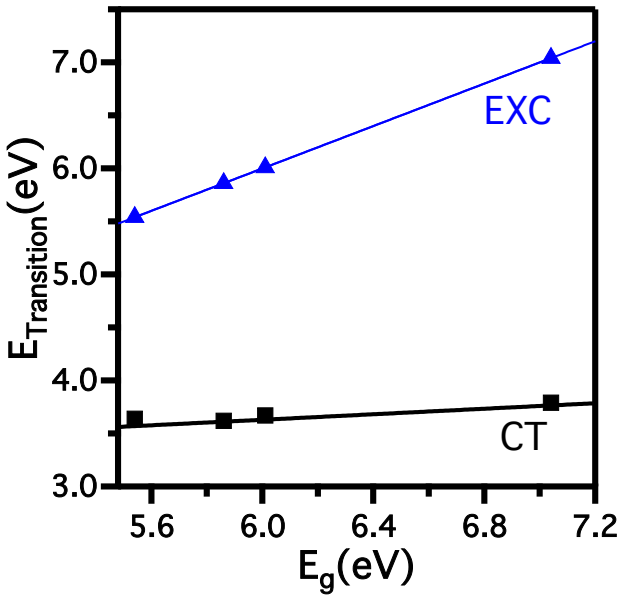

FIG. 9. TD-B3LYP/6-31G(d) NV to CB excitation and excitonic transition, as a function of the band-to-band-excitonic transition, for the $^3NV^-$ systems. Extrapolation of the CT energies gives a value of 3.56 eV for the bulk and the ratio between ΔE_{CT} and ΔE_{EXC} as the slope of the linear fit is 0.13.

IV. CONCLUSION

Although standard orbital energy differences are able to provide a qualitative view of electronic excited states, they are incapable of describing NV-NV or CT electronic transitions in NV center doped nanodiamonds. In this work a combined (TD)DFT study and cluster approach is carried out on several nanodiamonds of different sizes exploring simultaneously the effect of the local NV center symmetry on the electronic structure and the size dependence of the CT transitions.

A splitting of 60 meV of mid-gap transitions is observed when NV is moved away from the C_{3v} center of the nanocrystal, comparable to the splitting obtainable by applying anisotropic lattice strain or introducing non-spherical shape of nanocrystals. Compared to electrons in the excitonic VB to CB transitions, electrons in the CT transitions in the NV-doped systems have greater effective mass due to the electron hole interaction involving the localized hole.

This work provides an important theoretical framework that can be extended to the characterization of other defects in nanodiamonds, providing new insights into possible mechanism for tuning the optical properties in these materials.

ACKNOWLEDGMENTS

This work was supported by the National Science Foundation (CHE-1464497 and CHE-1565520). The University of Washington Student Technology Fund is gratefully acknowledged. This work is further supported by the National Science Foundation Graduate Research Fellowship No. DGE-1256082 to J.J.G.

* xsli@uw.edu

[1] M. E. Levinshteĭn, S. L. Rumyantsev, and M. Shur, *Handbook Series on Semiconductor Parameters: Si, Ge, C (Diamond), GaAs, GaP, GaSb, InAs, InP, InSb* (World Scientific Publishing, Singapore, 1996).

[2] J. R. Chelikowsky, M. Alemany, T. Chan, and G. Dalpian, Rep. Prog. Phys. **74**, 046501 (2011).

[3] R. Beaulac, S. T. Ochsenbein, D. R. Gamelin, and V. Klimov, in *Nanocrystal Quantum Dots, Second Edition*, Vol. 2, edited by V. I. Klimov (CRC Press, Boca Raton,

FL, 2010) pp. 397–453.
[4] L. Canham, Nature **408**, 411 (2000).
[5] J. Chelikowsky, MRS Bull. **27**, 951 (2002).
[6] J. Chelikowsky, Mater. Today **5**, 64 (2002).
[7] J. R. Chelikowsky and M. L. Cohen, Phys. Rev. Lett. **32**, 674 (1974).
[8] C. Kittel and P. McEuen, *Introduction to solid state physics*, Vol. 8 (Wiley, New York, NY, 1976).
[9] N. Ashcroft and N. Mermin, *Solid State Physics* (Saunders College, Philadelphia, PA, 1976).
[10] L. E. Brus, J. Chem. Phys. **80**, 4403 (1984).
[11] M. G. Bawendi, M. L. Steigerwald, and L. E. Brus, Annu. Rev. Phys. Chem. **41**, 477 (1990).
[12] R. Beaulac, S. T. Ochsenbein, and D. R. Gamelin, in *Nanocrystal Quantum Dots*, edited by V. I. Klimov (Taylor & Francis, New York, 2010) Chap. Chapter 11. Colloidal Transition-Metal-Doped Quantum Dots, pp. 397–453, 2nd ed.
[13] D. Chadi, Phys. Rev. Lett. **72**, 534 (1994).
[14] G. F. Neumark, Mater. Sci. Eng. R-Rep. **21**, 1 (1997).
[15] M. C. Troparevsky and J. R. Chelikowsky, J. Chem. Phys. **114**, 943 (2001).
[16] A. Yoffe, Adv. Phys. **50**, 1 (2001).
[17] T.-L. Chan, M. L. Tiago, E. Kaxiras, and J. R. Chelikowsky, Nano Lett. **8**, 596 (2008).
[18] D. V. Melnikov and J. R. Chelikowsky, Phys. Rev. Lett. **92**, 046802 (2004).
[19] A. Ranjbar, M. Babamoradi, M. Heidari Saani, M. A. Vesaghi, K. Esfarjani, and Y. Kawazoe, Phys. Rev. B **84**, 165212 (2011).
[20] M. W. Doherty, N. B. Manson, P. Delaney, F. Jelezko, J. Wrachtrup, and L. C. L. Hollenberg, Phys. Rep. **528**, 1 (2013).
[21] N. B. Manson, K. Beha, A. Batalov, L. J. Rogers, M. W. Doherty, R. Bratschitsch, and A. Leitenstorfer, Phys. Rev. B **87**, 155209 (2013).
[22] N. Manson and J. Harrison, Diamond Relat. Mater. **14**, 1705 (2005).
[23] K. Holt, Phil. Trans. R. Soc. A **365**, 2845 (2007).
[24] G. Balasubramanian, I. Chan, R. Kolesov, M. Al-Hmoud, J. Tisler, C. Shin, C. Kim, A. Wojcik, P. Hemmer, A. Krueger, T.Hanke, A. Leitenstorfer, R. Bratschitsch, F. Jelezko, and J. Wrachtrup, Nature **455**, 648 (2008).
[25] Y.-R. Chang, H.-Y. Lee, K. Chen, C.-C. Chang, D.-S. Tsai, C.-C. Fu, T.-S. Lim, Y.-K. Tzeng, C.-Y. Fang, C.-C. Han, H.-C. Chang, and W. Fann, Nat. Nano. **3**, 284 (2008).
[26] L. McGuinness, Y. Yan, A. Stacey, D. Simpson, L. Hall, D. Maclaurin, S. Prawer, P. Mulvaney, J. Wrachtrup, F. Caruso, R. E. Scholten, and L. C. L. Hollenberg, Nat. Nano. **6**, 358 (2011).
[27] N. S. Norberg, G. M. Dalpian, J. R. Chelikowsky, and D. R. Gamelin, Nano Lett. **6**, 2887 (2006).
[28] E. Badaeva, C. M. Isborn, Y. Feng, S. T. Ochsenbein, D. R. Gamelin, and X. Li, J. Phys. Chem. C **113**, 8710 (2009).
[29] C. Bradac, T. Gaebel, N. Naidoo, M. Sellars, J. Twamley, L. Brown, A. Barnard, T. Plakhotnik, A. Zvyagin, and J. Rabeau, Nat. Nano. **5**, 345 (2010).
[30] F. M. Hossain, M. W. Doherty, H. F. Wilson, and L. C. L. Hollenberg, Phys. Rev. Lett. **101**, 226403 (2008).
[31] J. A. Larsson and P. P. Delaney, Phys. Rev. B **77**, 165201 (2008).
[32] A. Gali, M. Fyta, and E. Kaxiras, Phys. Rev. B **77**, 155206 (2008).
[33] A. Gali, E. Janzén, P. Deák, G. Kresse, and E. Kaxiras, Phys. Rev. Lett. **103**, 186404 (2009).
[34] P. Delaney, J. C. Greer, and J. A. Larsson, Nano Lett. **10**, 610 (2010).
[35] Y. Ma, M. Rohlfing, and A. Gali, Phys. Rev. B **81**, 041204 (2010).
[36] A. Gali, Phys. Status Solidi B **248**, 1337 (2011).
[37] V. M. Acosta, C. Santori, A. Faraon, Z. Huang, K.-M. C. Fu, A. Stacey, D. A. Simpson, K. Ganesan, S. Tomljenovic-Hanic, A. D. Greentree, S. Prawer, and R. G. Beausoleil, Phys. Rev. Lett. **108**, 206401 (2012).
[38] J. P. Goss, R. Jones, S. J. Breuer, P. R. Briddon, and S. Öberg, Phys. Rev. Lett. **77**, 3041 (1996).
[39] C.-K. Lin, Y.-H. Wang, H.-C. Chang, M. Hayashi, and S. H. Lin, J. Chem. Phys. **129**, 124714 (2008).
[40] A. S. Zyubin, A. Mebel, M. Hayashi, H. C. Chang, and S. H. Lin, J. Comput. Chem. **30**, 119 (2009).
[41] R. Beaulac, Y. Feng, J. W. May, E. Badaeva, D. R. Gamelin, and X. Li, Phys. Rev. B **84**, 195324 (2011).
[42] J. W. May, R. J. McMorris, and X. Li, J. Phys. Chem. Lett. **3**, 1374 (2012).
[43] J. W. May, J. Ma, E. Badaeva, and X. Li, J. Phys. Chem. C **118**, 13152 (2014).
[44] J. J. Goings, A. M. Schimpf, J. W. May, R. W. Johns, D. R. Gamelin, and X. Li, J. Phys. Chem. C **118**, 26584 (2014).
[45] B. Peng, J. W. May, D. R. Gamelin, and X. Li, J. Phys. Chem. C **118**, 7630 (2014).
[46] L. R. Bradshaw, J. W. May, J. L. Dempsey, X. Li, and D. R. Gamelin, Phys. Rev. B **89**, 115312 (2014).
[47] N. R. Greiner, D. S. Phillips, J. D. Johnson, and F. Volk, Nature , 440 (1988).
[48] V. Y. Dolmatov, Russ. Chem. Rev. **76**, 339 (2007).
[49] E. Ōsawa, Pure Appl. Chem. **80**, 1365 (2008).
[50] K. Takahashi, A. Yoshikawa, and A. Sandhu, *Wide bandgap semiconductors: fundamental properties and modern photonic and electronic devices* (Springer, New York, NY, 2007).
[51] M. J. Frisch, G. W. Trucks, H. B. Schlegel, G. E. Scuseria, M. A. Robb, J. R. Cheeseman, G. Scalmani, V. Barone, B. Mennucci, G. A. Petersson, H. Nakatsuji, M. Caricato, X. Li, H. P. Hratchian, A. F. Izmaylov, J. Bloino, G. Zheng, J. L. Sonnenberg, W. Liang, M. Hada, M. Ehara, K. Toyota, R. Fukuda, J. Hasegawa, M. Ishida, T. Nakajima, Y. Honda, O. Kitao, H. Nakai, T. Vreven, J. A. M. Jr., J. E. Peralta, F. Ogliaro, M. Bearpark, J. J. Heyd, E. Brothers, K. N. Kudin, V. N. Staroverov, T. Keith, R. Kobayashi, J. Normand, K. Raghavachari, A. Rendell, J. C. Burant, S. S. Iyengar, J. Tomasi, M. Cossi, N. Rega, J. M. Millam, M. Klene, J. E. Knox, J. B. Cross, V. Bakken, C. Adamo, J. Jaramillo, R. Gomperts, R. E. Stratmann, O. Yazyev, A. J. Austin, R. Cammi, C. Pomelli, J. W. Ochterski, R. L. Martin, K. Morokuma, V. G. Zakrzewski, G. A. Voth, P. Salvador, J. J. Dannenberg, S. Dapprich, P. V. Parandekar, N. J. Mayhall, A. D. Daniels, O. Farkas, J. B. Foresman, J. V. Ortiz, J. Cioslowski, and D. J. Fox, "Gaussian Development Version Revision H.13," Gaussian Inc., Wallingford CT 2012.
[52] A. D. Becke, J. Chem. Phys. **98**, 5648 (1993).
[53] C. Lee, W. Yang, and R. G. Parr, Phys. Rev. B **37**, 785 (1988).
[54] B. Miehlich, A. Savin, H. Stoll, and H. Preuss, Chem. Phys. Lett. **157**, 200 (1989).
[55] H. Iikura, T. Tsuneda, T. Yanai, and K. Hirao, J. Chem. Phys. **115**, 3540 (2001).

[56] A. D. Becke, Phys. Rev. A **38**, 3098 (1988).
[57] M. E. Casida, *Recent Advances in Density Functional Methods:(Part I)*, edited by D. P. Chong, Vol. 1 (World Scientific Publishing, Singapore, 1995) pp. 155–193.
[58] A. Dreuw and M. Head-Gordon, Chem. Rev. **105**, 4009 (2005).
[59] R. E. Stratmann, G. E. Scuseria, and M. J. Frisch, J. Chem. Phys. **109**, 8218 (1998).
[60] W. Liang, S. A. Fischer, M. J. Frisch, and X. Li, J. Chem. Theor. Comput. **7**, 3540 (2011).
[61] P. J. Lestrange, P. D. Nguyen, and X. Li, J. Chem. Theor. Comput. **11**, 2994 (2015).
[62] S. Vepřek, Thin Solid Films **297**, 145 (1997).
[63] E. Badaeva, Y. Feng, D. R. Gamelin, and X. Li, New J. Phys. **10**, 055013 (2008).
[64] L. E. Brus, J. Chem. Phys. **79**, 5566 (1983).
[65] L. Brus, J. Phys. Chem. **90**, 2555 (1986).
[66] G. Davies and M. F. Hamer, Proc. R. Soc. London, Ser. A **348**, 285 (1976).
[67] B. Deng, R. Q. Zhang, and X. Q. Shi, Sci. Rep. **4**, 5144 (2014).
[68] J. R. Weber, W. F. Koehl, J. B. Varley, A. Janotti, B. B. Buckley, C. G. Van de Walle, and D. D. Awschalom, Proc. Natl. Acad. Sci. U.S.A. **107**, 8513 (2010).
[69] K. C. Fu, C. Santori, P. E. Barclay, L. J. Rogers, N. B. Manson, and R. G. Beausoleil, Phys. Rev. Lett. **103**, 256404 (2009).
[70] M. W. Doherty, V. V. Struzhkin, D. A. Simpson, L. P. McGuinness, Y. Meng, A. Stacey, T. J. Karle, R. J. Hemley, N. B. Manson, L. C. L. Hollenberg, and S. Prawer, Phys. Rev. Lett. **112**, 047601 (2014).
[71] N. B. Manson, J. P. Harrison, and M. J. Sellars, Phys. Rev. B **74**, 104303 (2006).